Coupled Systems Mechanics, *Vol. 14, No. 6 (2025) 595-619*
https://doi.org/10.12989/csm.2025.14.6.595

Coupled buckling behavior of two-directional coated functionally graded nanobeams resting on Winkler-Pasternak-Kerr foundations

Ahmed Amine Daikh*[1,2], Aicha Remil[2], Aicha Bessaim[2,3], Meriem Sahla[2], Mohammed Sid Ahmed Houari[2], Mohamed Oujedi Belarbi[4], Ahmed Drai[5,6], Mohamed Guerroudj[5] and Mohamed A. Eltaher[7,8]

[1]*Artificial Intelligence Laboratory for Mechanical and Civil Structures, and Soil, University of Naama, P.O. Box 66, 45000 Naama, Algeria*
[2]*Laboratoire d'Etude des Structures et de Mécanique des Matériaux, Département de Génie Civil, Faculté des Sciences et de la Technologie, Université Mustapha Stambouli, B.P. 305, 29000 Mascara, Algeria*
[3]*Faculty of Architecture and Civil Engineering, USTO, BP 155, Oran El Mnaoer, Oran, Algeria*
[4]*Laboratoire de Recherche en Génie Civil, LRGC, Université de Biskra, B.P. 145, 07000 Biskra, Algeria*
[5]*Laboratory of Applied Biomechanics and Biomaterials, EN Oran, BP1513 El Mnaour, 31000 Oran, Algeria*
[6]*Department of Mechanical Engineering, University of Mustapha Stambouli, Mascara, Algeria*
[7]*Mechanical Design and Production Department, Faculty of Engineering, Zagazig University, P.O. Box 44519, Zagazig, Egypt*
[8]*Mechanical Engineering Department, Faculty of Engineering, King Abdulaziz University, P.O. Box 80204, Jeddah, Saudi Arabi*

(Received November 5, 2025, Revised January 2, 2026, Accepted January 20, 2026)

Abstract. A novel refined shear deformation theory with three variables is proposed to investigate the buckling behavior of two-directional coated functionally graded nanobeams. The displacement field is formulated based on the principles of Euler-Bernoulli beam theory. This study examines two distinct categories of coated functionally graded nanobeams: Hardcore and Softcore nanobeams. Three material distribution patterns are considered: a bidirectional configuration, a unidirectional transverse distribution, and a unidirectional axial arrangement. The strain gradient nonlocal elasticity theory is implemented to account for small-scale effects. The equilibrium equations governing nanobeams are derived using the total potential energy principle. A refined solution approach, leveraging Galerkin's method, addresses various boundary conditions efficiently. The functionally graded beam is modelled on an elastic foundation described by the Winkler, Pasternak, and Kerr models. The obtained results show that the buckling behavior of the coated nanobeams is significantly influenced by the coating layer's thickness, material properties, boundary conditions, and gradient distribution. We find that the two-directional coating configuration can improve buckling resistance and reduce sensitivity to loading direction compared to traditional one-directional coatings. The findings of this study have important implications for the design and optimisation of nanoscale structures and devices, particularly in applications where mechanical stability and reliability are critical, such as in nanoelectromechanical systems (NEMS) and nanoscale sensors.

Keywords: buckling; complex elastic foundation; small scale effect; two-directional FGM

*Corresponding author, Professor, E-mail: daikhresearch@gmail.com

 ISSN: 2234-2184 (Print), 2234-2192 (Online)

1. Introduction

Functionally Graded Materials (FGMs) constitute an advanced class of composite materials with a continuous and gradual variation in properties such as mechanical strength, thermal conductivity, and stiffness across their thickness. This spatial gradient eliminates abrupt property transitions thereby reducing stress concentrations and enhancing interfacial bonding key limitations of conventional laminated composites (Mouffoki *et al.* 2017, Bezzina *et al.* 2022, Houari *et al.* 2025).

Owing to these advantages, FGMs have been widely adopted in high-performance applications, particularly in aerospace, biomedical, and automotive industries, where superior mechanical reliability and thermal resistance are essential. However, structural components of FGMs often operate under extreme environmental conditions, including high temperatures and moisture exposure, which can significantly affect their stiffness and durability, especially at the nanoscale. Consequently, analysing nanoscale FGM structures subjected to thermal and hygrothermal effects has drawn significant research interest in recent years (Mouffoki *et al.* 2025, Drai *et al.* 2023, Rizov 2017).

Consequently, it is always important to use a fresh methodology to examine the behavior of such materials. According to the first-order shear deformation theory, the transverse shear stress components are assumed to be uniform across the plate thickness, thereby requiring a shear correction factor. To address the limitations of the first-order shear deformation theory (FSDT), higher-order shear deformation theories (HSDT) have been developed. These theories provide a more accurate representation of the displacement field and shear stress distribution through the thickness (Reddy 1984, Carrera 1999, Mohamed *et al.* 2025b).

Extensive research has examined advanced composite structures' static, vibrational, and buckling responses under various loading and boundary conditions. These studies underscore the growing relevance of functionally graded materials (FGMs) in engineering applications, owing to their ability to enhance structural performance by mitigating stress concentrations and optimizing mechanical properties. The continuous gradation of material constituents in FGMs enables improved stiffness-to-weight ratios, better resistance to thermal and mechanical loads, and increased durability compared to traditional laminated composites. As a result, understanding their behavior under different physical and environmental conditions remains a critical focus in the design and analysis of next-generation composite structures (Daikh *et al.* 2022, Ermis *et al.* 2024, Fang *et al.* 2019, Jamshidi *et al.* 2019, Karamanli 2023, Mohamed *et al.* 2024, Mohamed *et al.* 2025d, Remil *et al.* 2019, Turan and Adiyaman 2024, Xin and Kiani 2023).

Nanostructures, such as nanorods, nanobeams, and nanoplates, have garnered significant attention due to their exceptional mechanical, thermal, chemical, and electronic properties (Ekinci and Roukes 2005, Rahmani *et al.* 2017).These nanoscale components are essential in various applications, including micro/nano-electromechanical systems (MEMS/NEMS) and nanoactuators, driving progress in the modelling and analysis of micro- and nanoscale structures. However, as their characteristic dimensions decrease, size-dependent effects become more pronounced, significantly impacting their mechanical and physical behavior. The emergence of functionally graded nanomaterials has paved the way for developing advanced materials with enhanced performance and customisable properties (Belarbi *et al.* 2025, Vinh *et al.* 2022, Zghal and Dammak 2020).

Theoretical models play a fundamental role in capturing size-dependent effects on the mechanical behavior of nanostructures, particularly in static bending, free vibration, and buckling.

These effects are influenced by both internal material length scales and external structural dimensions, necessitating advanced modelling approaches for accurate analysis. For instance, Akgöz and Civalek (2012) employed a modified strain gradient theory to conduct static analyses of microbeams, highlighting the significance of higher-order stress gradients. Similarly, Li *et al.* (2015) analysed the flexural wave frequency response of functionally graded Euler-Bernoulli beams by employing nonlocal strain gradient theory, demonstrating the interplay between material gradation and nonlocal effects in wave propagation analysis. Karamanlı and Vo (2018) used quasi-3D theory and FEM for examining the flexural behavior of 2D FG microbeams under uniformly distributed load with different boundary conditions. Such studies highlight the necessity for advanced continuum theories to more accurately predict the mechanical behavior of nanostructures.

The study of functionally graded (FG) nanobeams has attracted considerable interest due to their potential applications in cutting-edge engineering structures. Various theoretical models have been developed to study their mechanical response under different loading and boundary conditions). Eltaher *et al.* (2013) investigated the stability and static behavior of nanobeams composed of functionally graded materials, highlighting the influence of material gradation, boundary conditions, and nonlocal effects on the bending behavior. Extending this work, Eltaher *et al.* (2014) formulated the governing equation for the free vibration of FG nanobeams and utilised the finite element method (FEM) to analyze their structural response. In parallel, Kolahchi *et al.* (2015) conducted bending analysis of FG nanoplates using a novel sinusoidal shear deformation theory, Meanwhile, Xu *et al.* (2017) investigated the bending and buckling behavior of Euler-Bernoulli beams under the framework of nonlocal strain gradient theory. Higher-order shear deformation theories (HSDTs) have been developed to better capture shear deformation effects, ensuring zero shear stress conditions at beam surfaces without requiring shear correction factors. Based on quasi-3d shear deformation theory , Karamanlı (2017) studied bending of two directional functionally graded sandwich beams, further, the third-order shear deformation theory is employed to analyse free vibration under diffrent boundary conditions (Karamanlı 2018).

Nonlocal elasticity theory has been extensively adopted to model the behavior of FG nanostructures accurately. This theory effectively captures size-dependent effects that become significant at the nanoscale, leading to a more precise prediction of mechanical responses (Belarbi *et al.* 2025). Nonlocal beam and plate models have been employed to investigate the static, vibrational, and buckling behaviors of both homogeneous and functionally graded structures (Belkacem *et al.* 2023, Daikh *et al.* 2021, Ladmek *et al.* 2023, Nguyen *et al.* 2025). In particular, the buckling response of FG nanobeams is significantly influenced by material property gradients, geometric configurations, and loading conditions. Material heterogeneity affects stiffness and strength, while geometric parameters such as length, thickness, and boundary conditions play a crucial role in stability determination. External loads, including axial forces and moments, further complicate the buckling behavior, necessitating sophisticated analytical models for accurate predictions (Daikh *et al.* 2023).

Several recent studies have advanced the understanding of FG nanostructures by incorporating additional complexities. Belarbi *et al.* (2022) the free vibration response of FG nanoplates was examined using a finite element model based on the layerwise theory and Eringen's nonlocal elasticity theory, effectively capturing small-scale effects. Further research has explored the mechanical performance of FG porous structures, carbon nanotube-reinforced composites (CNTRCs), and bidirectional functionally graded materials (2D-FGMs) under diverse boundary conditions and loading scenarios. For instance, Chen *et al.* (2020) performed a nonlinear free

vibration analysis of rotating 2D-FG porous microbeams using isogeometric analysis, while Remil *et al*. (2023) investigated the bending and dynamic stability of FG-CNTRC nanoplates. Turan *et al.* (2025) studied the static of bi-directional FG beams by Introduces an efficient and highly accurate shear-deformable finite element model .Additionally, higher-order shear deformation theories and quasi-3D models have enhanced the accuracy of theoretical predictions, facilitating more precise evaluations of static deformation, free vibration, and buckling behaviors of FG porous micro/nanostructures (Chen *et al.* 2023, Ebrahimi and Barati 2018, Karamanli and Vo 2021, Karamanli *et al*. 2023, Karamanli 2023, Sayyad *et al.* 2023, Mohamed *et al*. 2025c, Mohamed *et al*. 2025a, Tharwan *et al*. 2025, Yang *et al*. 2018). Despite these advancements, there remains a need for refined theoretical models capable of accurately capturing the complex behavior of FG nanobeams, particularly under combined mechanical and environmental loadings. This paper aims to address this gap by proposing a three-variable refined shear deformation theory with an integrated correction factor framework. The proposed model incorporates transverse shear strains that vary quadratically through the beam thickness, offering a comprehensive representation of buckling mechanisms. By integrating nonlocal elasticity theory, the model effectively captures size-dependent effects essential for nanoscale analysis. Moreover, the framework accommodates unidirectional, bidirectional, and tridirectionally functionally graded configurations.

The primary objective of this study is to develop a novel solution approach based on the Galerkin method to investigate the buckling behavior of two-directional functionally graded beams resting on elastic foundations modeled by Winkler, Pasternak, and Kerr theories. This approach is expected to improve the accuracy and reliability of buckling predictions, ultimately contributing to the optimal design of advanced FG nanostructures.

2. Mathematical formulation

The main focus of this study is the analysis of FG-coated beams, as illustrated in Fig. 1. These beams have predefined dimensions for length and thickness, denoted as "$L\times h$".

2.1 Functionally graded materials

The functionally graded (FG) composite beam consists of metal and ceramic phases, with the volume fraction of each constituent varying in two directions. The study focuses on two types of FG beams: hardcore and softcore. It also looks at three different patterns of CNT distribution: "2D-FG", which is a two-way material distribution pattern; "T-FG", which is a one-way transverse material distribution pattern; and "A-FG", which is a one-way axial material distribution pattern. The law of mixture serves as a fundamental basis to accurately calculate the properties of materials. To simplify the analysis, Poisson's ratio "ν" is assumed to be constant. Young's modulus "E" can be expressed as follows (Yamanouti *et al.* 1990)

$$E(x,z) = E_m + (E_c - E_m)V(x,z) \tag{1}$$

The given equation comprises two components: one corresponding to the Young's modulus (E_m) of the metallic phase and the other to the Young's modulus (E_c) of the ceramic phase. Two functions govern the volume fraction, each corresponding to a specific direction. These functions describe the volume fraction variation concerning each direction within the composite material

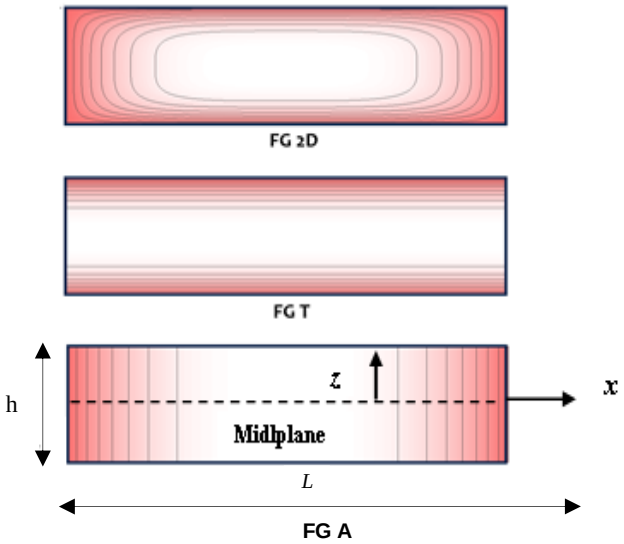

Fig. 1 Geometry and schemes of the FG beam

Ghandourah *et al*. (2023).

$$V(x)=\left|\left(\frac{|2x-a|}{a}\right)^{k}-1\right|$$
$$V(z)=\left|\left(\frac{|2z|}{h}\right)^{p}-1\right| \tag{2}$$

The total volume fraction of the Hardcore (HC) coated functionally graded (FG) beam is defined by the following expression

$$V(x,z)=V(x)V(z) \tag{3}$$

and for the Softcore (SC) coated FG beam

$$V(x,z)=1-V(x)V(z) \tag{4}$$

2.2 Nonlocal elasticity theory

Eringen (1983) nonlocal elasticity theory holds that strains at all body locations determine stress at a specific point x in an elastic continuum. Eringen's proposes the nonlocal stress tensor at a point "x".

Considering the influences of strain gradient stress and nonlocal elastic stress, the constitutive equation governing the behavior of the nanoshell can be formulated as Lim *et al*. (2015)

$$\sigma_{ij}=\sigma_{ij}^{(0)}-\frac{d\sigma_{ij}^{(1)}}{dx} \tag{5}$$

The stress $\sigma_{ij}^{(0)}$ and the higher-order stress $\sigma_{ij}^{(1)}$ are dependent on the strain ε_{kl} and the first-order strain gradient $\varepsilon_{kl,x}$, and they can be written as

$$\sigma_{ij}^{(0)} = \int_0^L C_{ijkl}\alpha_0(x,x',e_0a)\varepsilon_{kl}(x')dx' \tag{6}$$

$$\sigma_{ij}^{(1)} = l^2\int_0^L C_{ijkl}\alpha_1(x,x',e_1a)\varepsilon_{kl}(x')dx' \tag{7}$$

In the context of strain gradient and nonlocal elasticity theories, C_{ijkl} ae elastic constants, l represents the material length scale parameter, which describes the field of the strain gradient stress. The nonlocal parameters, which describe the field of the nonlocal elastic stress, are e_0a and e_1a, and $\alpha_0(x,x',e_0a)$ and $\alpha_1(x,x',e_1a)$ are the nonlocal kernel functions. The constitutive relation incorporating these factors can be expressed as

$$\left[1-\left(e_1a\right)^2\nabla^2\right]\left[1-\left(e_0a\right)^2\nabla^2\right]\sigma_{ij} = C_{ijkl}\left[1-\left(e_1a\right)^2\nabla^2\right]\varepsilon_{kl} - C_{ijkl}l^2\left[1-\left(e_0a\right)^2\nabla^2\right]\nabla^2\varepsilon_{kl} \tag{8}$$

The Laplacian operator ($\nabla^2 = \frac{\partial^2}{\partial x^2}$) is a second-order differential operator that measures the rate atwhich the average value of a function around a point differs from the value at that point.

Mathematically, it is defined as the divergence of the gradient of a scalar field. The nonlocal strain gradient constitutive relations, by assuming that $e = e_0 = e_1$, can be presented as (Lim 2015)

$$\left[1-\mu\nabla^2\right]\sigma_{ij} = C_{ijkl}\left[1-\lambda\nabla^2\right]\varepsilon_{kl} \tag{9}$$

Where $\mu = (ea)^2$ is the nonlocal parameter that is defined as $\mu = (ea)^2$ and $\lambda = l^2$.

2.3 Displacement field

To derive the governing equations for coated functionally graded (FG) nanobeams, a shear deformation theory based on a hyperbolic sine function (HSBT) is utilised. The proposed displacement field is formulated using the Euler-Bernoulli beam theory (EBT) and includes a correction factor to account for the effects of thickness stretching. This model involves three unknowns, which is notably fewer than other quasi-3D theories that generally require four or more unknowns.

$$\begin{aligned} u(x,z) &= u_0 - z\frac{\partial w_0}{dx} - \phi(z)\frac{\partial^3 w_0}{dx^3} \\ w(x,z) &= w_0 + g(z)\psi_0 \end{aligned} \tag{10}$$

$$\begin{aligned} \phi(z) &= Kf(z) \\ g(z) &= \frac{\partial\phi(z)}{\partial z} \end{aligned} \tag{11}$$

In Euler-Bernoulli beam theory, rotational inertia and shear deformation are entirely neglected. The displacement field based on Euler-Bernoulli beam is determined by assuming that set $\phi(z) = g(z) = 0$, and u_0 and w_0 are the curved axial and transverse displacements of the midline of the beam, respectively. ψ_0 is the shear components of the deflection The hyperbolic sine function is $f(z) = h\sinh(z/h) - 3z^3/2h^2$. The correction factor, κ, is determined by solving the stiffness matrix determinant.

It is essential to highlight that the additional component $g(z)\psi_0$ in Eq. (11) has been introduced to study the impact of thickness stretching on static behavior.

The strain components related to the displacement field, derived concerning the curvilinear covariant basis vector, are obtained as

$$\begin{aligned} \varepsilon_x &= \frac{\partial u}{dx} = \frac{\partial u_0}{dx} - z\frac{\partial^2 w_0}{dx^2} - \phi(z)\frac{\partial^4 w_0}{dx^4} \\ \varepsilon_z &= \frac{\partial w}{dz} = \frac{\partial g(z)}{dz}\psi_0 \\ \gamma_{xz} &= \frac{\partial u}{dz} + \frac{\partial w}{dx} = g(z)\left[-\frac{\partial^3 w_0}{dx^3} + \frac{\partial \psi_0}{\partial x}\right] \end{aligned} \tag{12}$$

2.4 Constitutive equations

The linear constitutive relations, considering the effect of thickness stretching, are expressed as (Daikh *et al*. 2022)

$$\left[1-\mu\nabla^2\right]\begin{Bmatrix}\sigma_x\\ \sigma_z\\ \tau_{xz}\end{Bmatrix} = \left[1-\lambda\nabla^2\right]\begin{bmatrix}Q_{11} & Q_{13} & 0\\ Q_{13} & Q_{33} & 0\\ 0 & 0 & Q_{55}\end{bmatrix}\begin{Bmatrix}\varepsilon_x\\ \varepsilon_z\\ \gamma_{xz}\end{Bmatrix} \tag{13}$$

Where

$$\begin{aligned} Q_{11} = Q_{33} &= \frac{E(x,z)}{1-\upsilon^2} \\ Q_{13} &= \frac{\upsilon E(x,z)}{1-\upsilon^2} \\ Q_{55} &= \frac{E(x,z)}{2(1+\upsilon)} \end{aligned} \tag{14}$$

When the thickness stretching effect is neglected ($\varepsilon_z = 0$), the elastic constants Q_{ij} are simplified as follows

$$\begin{aligned} Q_{11} = Q_{33} &= E(x,z) \\ Q_{13} &= 0 \\ Q_{55} &= \frac{E(x,z)}{2(1+\upsilon)} \end{aligned} \tag{15}$$

2.5 Variational formulation

To derive the equilibrium equations, the principle of potential energy is applied, where

$$\int \delta(U_P + U_F + U_E)dt = 0 \tag{16}$$

In the given equation, δ represents a variation. At the same time, U_P, U_E and U_F respectively denote the strain energy, the work done by the external axial force, and the additional strain energy induced by the elastic foundations.

The virtual strain energy of the beam is calculated as

$$\delta U_P = \int (\sigma_x \delta\varepsilon_x + \sigma_y \delta\varepsilon_y + \tau_{xz}\delta\gamma_{xz})dx \tag{17}$$

The work done by the axially compressive force "N_{xx}^0" can be represented as

$$\delta U_E = -\int N_{xx}^0 \frac{\partial w_0}{\partial x} + \frac{\partial \delta w_0}{\partial x} dx \tag{18}$$

The strain energy induced by elastic foundations can be defined as follows

$$\delta U_F = \int \left[U_{Winkler} + U_{Pasternak} + U_{Kerr}\right]dx \tag{19}$$

$$\delta U_F = \left(q_{Winkler} + q_{Pasternak} + q_{Kerr}\right) \tag{20}$$

In the given equation, the subscript represents the specific foundation model. The effectiveness of these proposed foundation models, which are based on a quasi-3D beam theory, will be discussed in detail below.

2.5.1 Winkler foundation model

The distributed load for a Winkler foundation model can be written as follows

$$q_{Winkler} = K_w\left[w_0 + g(z)\psi_0\right] \tag{21}$$

2.5.2 Pasternak foundation model

The distributed load in the Pasternak foundation model, which includes the Winkler parameter (K_w), and the shear layer parameter (K_g) can be described as follows

$$q_{Pasternak} = K_w\left[w_0 + g(z)\psi_0\right] - K_g\nabla^2\left[w_0 + g(z)\psi_0\right] \tag{22}$$

2.5.3 Kerr foundation model

The distributed reaction for the Kerr foundation model can be expressed as follows, a three-parameter elastic model that includes the shear layer parameter (K_s), upper elastic layer parameter (K_u), and lower elastic layer parameter (K_l).

$$q_{Kerr} = \left(\frac{k_l k_u}{k_l + k_u}\right)\left[w_0 + g(z)\psi_0\right] - \left(\frac{k_s k_u}{k_l + k_u}\right)\nabla^2\left[w_0 + g(z)\psi_0\right] \tag{23}$$

2.5 Governing equations

The governing equations for the current quasi-3D HSDT are determined for the static analysis by integrating the outcomes of Eqs. (12)-(13) insertion into Eq. (16). Therefore, by collecting the coefficients of δu_0, δw_0 and $\delta \psi_0$ and setting them equal to zero, the following equilibrium equations are derived. Consequently, the equilibrium equations for the FG beam can be expressed as

$$\begin{aligned}
&\delta u_0 : \frac{\partial N_x}{\partial x} = 0 \\
&\delta w_0 : \frac{\partial^2 M_x}{\partial x^2} + \frac{\partial^4 S_x}{\partial x^4} - \frac{\partial^3 V_{xz}}{\partial x^3} + N_{xx}^0 \frac{\partial^2 w}{\partial x^2} = 0 \\
&\delta \psi_0 : \frac{\partial V_{xz}}{\partial x} - Q_z = 0
\end{aligned} \tag{24}$$

The stress resultants in terms of the normal force "N_x", bending moment "M_x", higher-order generalised force "S_x", shear force "V_{xz}" and the additional stress couples Q_z, are defined as follows.

$$\left\{N_x, M_x, S_x\right\} = \int_{-h/2}^{h/2} \int_0^L \sigma_x \left\{1, z, \phi(z)\right\} dxdz \tag{25}$$

$$Q_z = \int_{-h/2}^{h/2} \int_0^L \left[\sigma_z \frac{\partial g(z)}{dz} \right] dxdz \tag{26}$$

$$V_{xz} = \int_{-h/2}^{h/2} \int_0^L \left[\tau_{xz} g(z)\right] dxdz \tag{27}$$

Eqs. (12)-(13) can be substituted into Eqs. (25)-(27) to obtain the stress resulting expressions as follows

$$N_x = A_{11} \frac{\partial u_0}{\partial x} - B_{11} \frac{\partial^2 w_0}{\partial x^2} - B_{11}^s \frac{\partial^4 w_0}{\partial x^4} + G_{12}^a \psi_0 \tag{28}$$

$$M_x = B_{11} \frac{\partial u_0}{\partial x} - D_{11} \frac{\partial^2 w_0}{\partial x^2} - D_{11}^s \frac{\partial^4 w_0}{\partial x^4} + H_{12} \psi_0 \tag{29}$$

$$S_x = B_{11}^s \frac{\partial u_0}{\partial x} - D_{11}^s \frac{\partial^2 w_0}{\partial x^2} - H_{11}^s \frac{\partial^4 w_0}{\partial x^4} + H_{12}^a \psi_0 \tag{30}$$

$$Q_z = G_{12}^a \frac{\partial u_0}{\partial x} - H_{12} \frac{\partial^2 w_0}{\partial x^2} - H_{12}^a \frac{\partial^4 w_0}{\partial x^4} + K_{22} \psi_0 \tag{31}$$

$$V_{xz} = -K_{33}^{s}\frac{\partial^3 w_0}{\partial x^3} + K_{33}^{s}\frac{\psi_0}{\partial x} \tag{32}$$

It is possible to compute the stiffness coefficients as

$$\left\{A_{11}, B_{11}, D_{11}, B_{11}^{s}, D_{11}^{s}, H_{11}^{s}\right\} = \int_{-h/2}^{h/2}\int_{0}^{L}\left[Q_{11}\left\{1, z, z^2, \phi(z), z\phi(z), \phi(z)^2\right\}\right]dxdz \tag{33}$$

$$\left\{G_{12}^{a}, H_{12}, H_{12}^{a}\right\} = \int_{-h/2}^{h/2}\int_{0}^{L}\left[Q_{13}\left\{\frac{dg(z)}{dz}, z\frac{dg(z)}{dz}, \phi(z)\frac{dg(z)}{dz}\right\}\right]dxdz \tag{34}$$

$$K_{22}^{a} = \int_{-h/2}^{h/2}\int_{0}^{L}\left[Q_{33}\left(\frac{dg(z)}{dz}\right)^2\right]dxdz \tag{35}$$

$$K_{33}^{a} = \int_{-h/2}^{h/2}\int_{0}^{L}\left[Q_{55}g(z)^2\right]dxdz \tag{36}$$

The governing equations in terms of generalized displacements u_0, w_0 and ψ_0 can be expressed as follows

$$\left[1-\lambda\nabla^2\right]\left[A_{11}\frac{\partial^2 u_0}{\partial x^2} - B_{11}\frac{\partial^3 w_0}{\partial x^3} - B_{11}^{s}\frac{\partial^5 w_0}{\partial x^5} + G_{12}^{a}\frac{\partial \psi_0}{\partial x}\right] = 0 \tag{37}$$

$$\begin{aligned}\left(1-\lambda\nabla^2\right)&\left[\begin{array}{c} B_{11}\frac{\partial^3 u_0}{\partial x^3} + B_{11}^{s}\frac{\partial^5 u_0}{\partial x^5} - D_{11}\frac{\partial^4 w_0}{\partial x^4} \\ +\left(-2D_{11}^{s} + K_{33}^{a}\right)\frac{\partial^6 w_0}{\partial x^6} - H_{11}^{s}\frac{\partial^8 w_0}{\partial x^8} + H_{12}\frac{\partial^2 \psi_0}{\partial x^2} \\ +\left(H_{12}^{a} - K_{33}^{a}\right)\frac{\partial^4 \psi_0}{\partial x^4}\end{array}\right] \\ &+\left(1-\mu\nabla^2\right)\left[\bar{N}_{xx}^{0}\frac{\partial^2 w_0}{\partial x^2} + U_f\right] = 0\end{aligned} \tag{38}$$

$$\left(1-\lambda\nabla^2\right)\left[\begin{array}{c} -G_{12}^{a}\frac{\partial u_0}{\partial x} + H_{12}\frac{\partial^2 w_0}{\partial x^2} + \left(H_{12}^{a} - K_{33}^{a}\right)\frac{\partial^4 w_0}{\partial x^4} \\ -K_{22}\psi_0 + K_{33}^{a}\frac{\partial^2 \psi_0}{\partial x^2}\end{array}\right] \tag{39}$$

3. Galerkin's method

In this analysis, we introduce a novel analytical solution for Eqs. (37)-(39) using Galerkin's

method for uniform nanobeams. The suggested solution technique is simple and effective for analysing nanobeams under various boundary conditions. In general, each edge of the nanobeam may be supported "S", clamped "C" or free "F". The generalised displacements can be expressed in the following form: Ghandourah *et al*. (2022)

$$u_0 = \sum_{m=1}^{\infty} U_m \frac{\partial X_m(x)}{\partial x}$$
$$w_0 = \sum_{m=1}^{\infty} W_m X_m(x) \tag{40}$$
$$\psi_0 = \sum_{m=1}^{\infty} \psi_m X_m(x)$$

Where U_m, W_m and ψ_m.are arbitrary parameters. m is the mode-shape number. The function $X_m(x)$ satisfies the aforementioned boundary conditions and can be defined in the following:

Hinged-Hinged (SS): $\alpha = m\pi/L$ and $X_m(x) = sin(\alpha x)$.

Clamped-Clamped (CC): $\alpha = 2m\pi/L$ and $X_m(x) = \frac{[1-cos(\alpha x)]}{2}$.

Clamped- Hinged: (CS): $\alpha = m\pi/L$ and $X_m(x) = sin(\alpha x)[1 - cos(\alpha x)]$.

Clamped-Free (CF): $\alpha = (2m-1)\pi/2L$ and $X_m(x) = cos(\alpha x)$.

By substituting Eq. (41) into Eqs. (38)-(40), one obtains

$$\begin{bmatrix} L_{11} & L_{12} & L_{13} \\ L_{21} & L_{22} & L_{23} \\ L_{31} & L_{32} & L_{33} \end{bmatrix} \begin{bmatrix} U_m \\ W_m \\ \psi_m \end{bmatrix} = \begin{Bmatrix} 0 \\ 0 \\ 0 \end{Bmatrix} \tag{41}$$

where $[L]$ is the matrix of the rigidity. The elements L_{ij} of $[L]$ can be written as

$$L_{11} = A_{11}\left(\int_0^L \frac{\partial^3 X_m}{\partial x^3}\frac{\partial X_m}{X_m}dx - \lambda\int_0^L \frac{\partial^5 X_m}{\partial x^5}\frac{\partial X_m}{X_m}dx\right) \tag{42}$$

$$L_{12} = -B_{11}\left(\int_0^L \frac{\partial^3 X_m}{\partial x^3}\frac{\partial X_m}{X_m}dx - \lambda\int_0^L \frac{\partial^5 X_m}{\partial x^5}\frac{\partial X_m}{X_m}dx\right) - B_{11}^s\left(\int_0^L \frac{\partial^5 X_m}{\partial x^5}\frac{\partial X_m}{X_m}dx - \lambda\int_0^L \frac{\partial^7 X_m}{\partial x^7}\frac{\partial X_m}{X_m}dx\right) \tag{43}$$

$$L_{13} = G_{12}^a\left(\int_0^L \frac{\partial X_m}{\partial x}\frac{\partial X_m}{\partial x}dx - \lambda\int_0^L \frac{\partial^3 X_m}{\partial x^3}\frac{\partial X_m}{X_m}dx\right) \tag{44}$$

$$L_{21} = B_{11}\left(\int_0^L \frac{\partial^4 X_m}{\partial x^4} X_m\, dx - \lambda \int_0^L \frac{\partial^6 X_m}{\partial x^6} X_m dx\right) + B_{11}^s\left(\int_0^L \frac{\partial^6 X_m}{\partial x^6} X_m\, dx - \lambda \int_0^L \frac{\partial^8 X_m}{\partial x^8}\frac{\partial X_m}{X_m} dx\right) \tag{45}$$

$$L_{22} = -\left(D_{11} - 2\frac{B_{11}^s}{R}\right)\left(\int_0^L \frac{\partial^4 X_m}{\partial x^4} X_m\, dx - \lambda \int_0^L \frac{\partial^6 X_m}{\partial x^6} X_m dx\right) - (2D_{11}^s - K_{33}^a)\left(\int_0^L \frac{\partial^6 X_m}{\partial x^6} X_m\, dx - \lambda \int_0^L \frac{\partial^8 X_m}{\partial x^8} X_m dx\right) - H_{11}^s\left(\int_0^L \frac{\partial^8 X_m}{\partial x^8} X_m\, dx - \lambda \int_0^L \frac{\partial^{10} X_m}{\partial x^{10}} X_m dx\right) - \left(k_w + \left(\frac{k_l k_u}{k_l + k_u}\right)\right)\left(\int_0^L X_m X_m\, dx - \mu \int_0^L \frac{\partial^2 X_m}{\partial x^2} X_m dx\right) + \left(k_g + \left(\frac{k_s k_u}{k_l + k_u}\right) - N_x^0\right)\left(\int_0^L \frac{\partial^2 X_m}{\partial x^2} X_m\, dx - \mu \int_0^L \frac{\partial^4 X_m}{\partial x^4} X_m dx\right) \tag{46}$$

$$L_{23} = H_{12}\left(\int_0^L \frac{\partial^2 X_m}{\partial x^2} X_m\, dx - \lambda \int_0^L \frac{\partial^4 X_m}{\partial x^4} X_m dx\right) (H_{12}^a - K_{33}^a) + \left(\int_0^L \frac{\partial^4 X_m}{\partial x^4} X_m\, dx - \mu \int_0^L \frac{\partial^6 X_m}{\partial x^6} X_m dx\right) \tag{47}$$

$$L_{31} = -G_{12}^a\left(\int_0^L \frac{\partial^2 X_m}{\partial x^2} X_m\, dx - \lambda \int_0^L \frac{\partial^4 X_m}{\partial x^4} X_m dx\right) \tag{48}$$

$$L_{32} = H_{12}\left(\int_0^L \frac{\partial^2 X_m}{\partial x^2} X_m\, dx - \lambda \int_0^L \frac{\partial^4 X_m}{\partial x^4} X_m dx\right) + (H_{12}^a - K_{33}^a)\left(\int_0^L \frac{\partial^4 X_m}{\partial x^4} X_m\, dx - \lambda \int_0^L \frac{\partial^6 X_m}{\partial x^6}\frac{\partial X_m}{X_m} dx\right) \tag{49}$$

$$L_{33} = K_{33}^{a}\left(\int_0^L \frac{\partial^2 X_m}{\partial x^2} X_m\, dx - \lambda \int_0^L \frac{\partial^4 X_m}{\partial x^4} X_m dx\right) - K_{22}^{a}\left(\int_0^L X_m X_m\, dx - \lambda \int_0^L \frac{\partial^2 X_m}{\partial x^2} X_m dx\right) \quad (50)$$

4. Results

This section examines the buckling behavior of FG nanobeams by analysing the dimensionless critical buckling load. The Young's modulus of the FG nanobeam varies in two directions, following the power-law homogenisation model. The material composition consists of a composite blend of aluminium as the metallic phase ($E_m = 70$ GPa) and alumina as the ceramic phase ($E_c =$ 380 GPa), while the Poisson's ratio remains constant at $\upsilon = 0.3$. The critical buckling load of functionally graded (FG) beams is expressed in the following dimensionless form

$$\overline{N} = \frac{12L}{E_m h^3} N_x^0 \quad (51)$$

4.1 Validation study

This section focuses on validating the proposed analytical approach to ensure its numerical efficiency and accuracy. To assess the reliability of the quasi-3D three-variable model, a comparative analysis is performed between the present mechanical buckling results and those reported in the literature. The computational findings are derived for power-law functionally graded beams (P-FGM), where the volume fraction distribution follows $V(z) = (0.5 + z/h)^p$.

In Table 1, the effectiveness of the proposed higher-order beam theory (HBT) is assessed by incorporating the thickness stretching effect ($\varepsilon_z \neq 0$) and comparing the results with those from the third-order shear deformation beam theory by Vo *et al.* (2014), Trinh *et al.* (2016) (TBT: $f(z) = z - 4z^3/3h^2$), as well as the sinusoidal shear deformation beam theory by Trinh *et al.* (2016) (SBT: SBT: $f(z) = h/\pi \sin(\pi z/h)$). This comparison serves to validate the accuracy and effectiveness of the proposed solution methodology. The results demonstrate a strong correlation with existing findings, confirming the reliability and precision of the present approach.

4.2 Parametric study

4.2.1 Correction factor variation

The correction factor "*K*" varies depending on the material distribution within the beam, as

Table 1 Dimensionless critical buckling load of FG beam ($\upsilon_c = \upsilon_m = 0.23$)

Ref.	p=0	p=1	p=2	p=5	p=10
Vo *et al.* (2014) (TBT)	49.5901	25.2116	19.6124	16.0842	14.4116
Trinh *et al.* (2016) (TBT)	49.6154	25.2248	19.6219	16.0910	14.4177
Trinh *et al.* (2016) (SBT)	49.6378	25.2306	19.6284	16.0833	14.4172
Present (HsBT)	49.5925	25.2108	19.6111	16.0837	14.4117

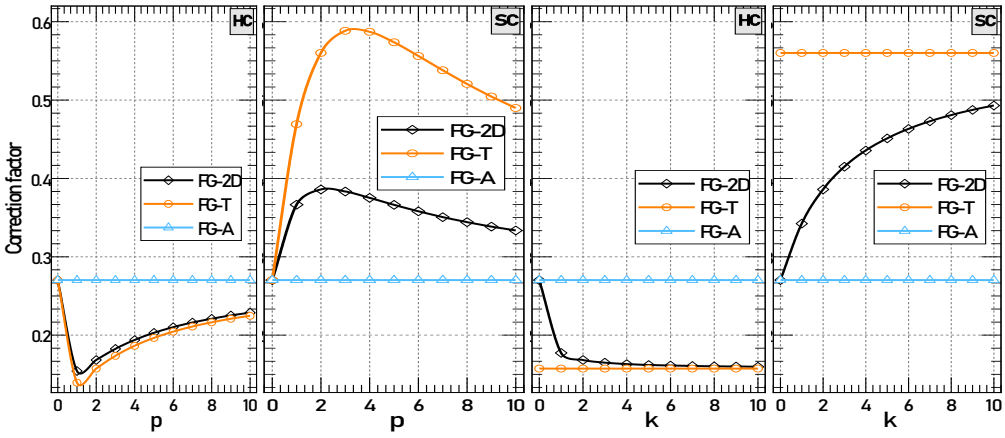

Fig. 2 Correction factor "κ" for different materials distributions

Table 2 Dimensionless buckling load versus the power-law indexes "p" and "k" (SS, L/h=5, μ=λ=0)

p	k	HC			SC		
		FG-2D	FG-T	FG-A	FG-2D	FG-T	FG-A
2	1	20.5907	26.2580	36.1079	37.3476	30.2750	22.6218
	2	23.8303	26.2580	43.8142	33.4874	30.2750	14.9155
	5	24.3699	26.2580	45.0986	32.8056	30.2750	13.6311
	10	24.7133	26.2580	45.9159	32.3636	30.2750	12.8137
6	1	27.6301	36.8567	36.1079	30.7449	20.6082	22.6218
	2	32.9028	36.8567	43.8142	25.1272	20.6082	14.9155
	5	33.7815	36.8567	45.0986	24.1583	20.6082	13.6311
	10	34.3406	36.8567	45.9159	23.5338	20.6082	12.8137
8	1	29.1922	39.2066	36.1079	29.2923	18.6158	22.6218
	2	34.9150	39.2066	43.8142	23.3244	18.6158	14.9155
	5	35.8687	39.2066	45.0986	22.3054	18.6158	13.6311
	10	36.4756	39.2066	45.9159	21.6509	18.6158	12.8137
10	1	30.2668	40.8224	36.1079	28.2849	17.2346	22.6218
	2	36.2988	40.8224	43.8142	22.0723	17.2346	14.9155
	5	37.3041	40.8224	45.0986	21.0184	17.2346	13.6311
	10	37.9438	40.8224	45.9159	20.3431	17.2346	12.8137

shown in Fig. 2. Notably, this factor is solely influenced by the beam's material properties. For isotropic beams, whether composed of ceramic or metal constituents, the correction factor remains constant at K=0.27. Additionally, the transverse variation in material composition plays a significant role in modifying the correction factor. However, when the material distribution is axial, the correction factor retains the same value as that of an isotropic material.

4.2.2 Material homogenization

Table 2 illustrates the influence of transverse and axial power-law parameters on the

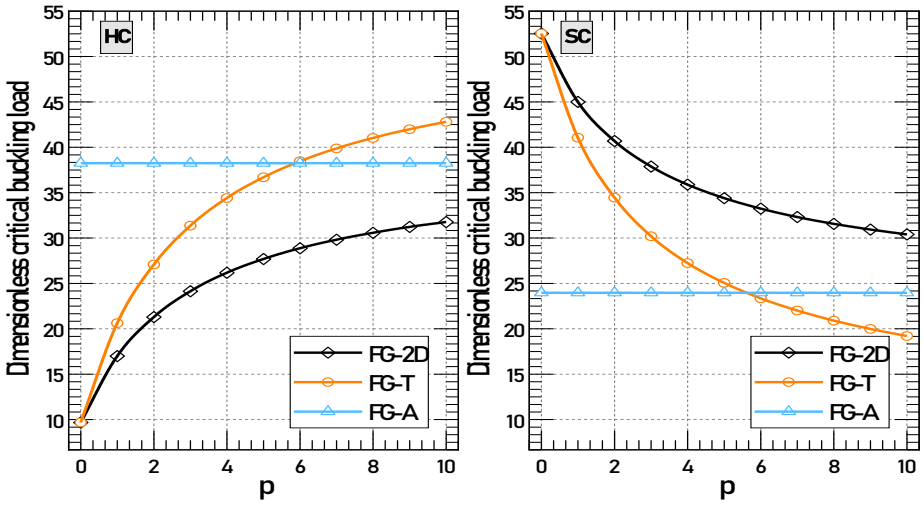

Fig. 3 Dimensionless buckling load versus the transverse power-law index "*p*" (SS, *k*=2, *L*/*h*=10, μ=λ=0)

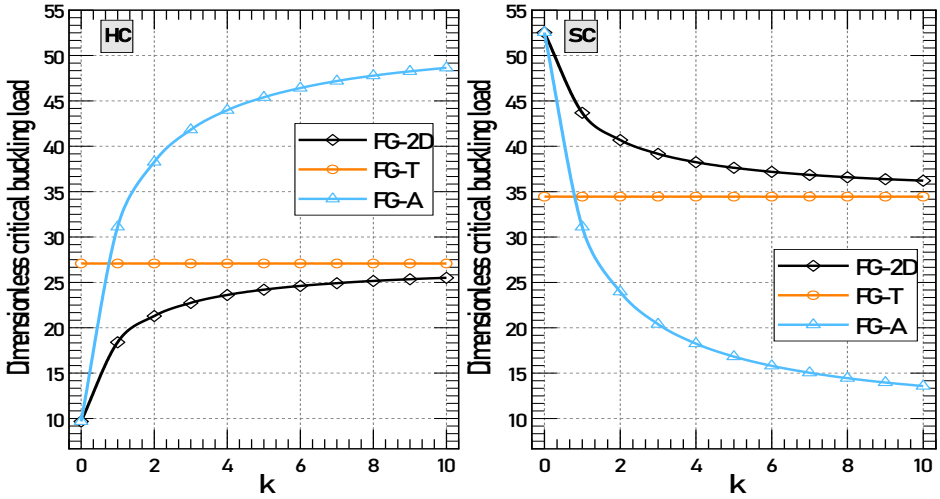

Fig. 4 Dimensionless buckling load versus the axial power-law index "*k*" (SS, *p*=2, *L*/*h*=10, μ=λ=0)

dimensionless critical buckling load of simply supported functionally graded (FG) beams. Additionally, Fig. 3 depicts the variation of the dimensionless buckling load as a function of the transverse power-law index "*p*". Notably, inthe FG-A configuration, where material properties vary only along the axial direction, changes in p have no impact, resulting in a constant buckling load regardless of whether the FG beam follows a Hardcore (HC) or Softcore (SC) scheme. Conversely, for Hardcore FG-2D and FG-T configurations, an increase in "*p*" enhances beam stiffness, necessitating higher loads to induce buckling. Among these, the FG-T configuration exhibits a greater sensitivity to changes in "*p*" compared to FG-2D. Fig. 4 illustrates the dimensionless buckling load as a function of the axial power-law index "*k*". Similar to the effect of the transverse power-law index "*p*", the FG-T beam remains unaffected by variations in "*k*", resulting in a constant critical buckling load. However, for other configurations, an increase in the

Table 3 Dimensionless buckling load versus the nonlocal parameter "μ" and length scale parameter "λ" (SS, L/h=5, μ=λ=0)

μ	λ	HC			SC		
		FG-2D	FG-T	FG-A	FG-2D	FG-T	FG-A
0.0	0.0	20.5907	26.2580	36.1079	37.3476	30.2750	22.6218
	0.25	22.6229	28.8495	39.6716	41.0337	33.2630	24.8545
	0.5	24.6551	31.4411	43.2353	44.7197	36.2510	27.0872
	0.75	26.6873	34.0327	46.7990	48.4058	39.2390	29.3198
	1.0	28.7195	36.6242	50.3627	52.0919	42.2270	31.5525
0.25	0.0	18.7410	23.8992	32.8643	33.9927	27.5553	20.5897
	0.25	20.5907	26.2580	36.1079	37.3476	30.2750	22.6218
	0.5	22.4403	28.6167	39.3514	40.7026	32.9946	24.6539
	0.75	24.2900	30.9755	42.5950	44.0575	35.7142	26.6860
	1.0	26.1396	33.3343	45.8386	47.4124	38.4338	28.7181
0.5	0.0	17.1962	21.9293	30.1554	31.1908	25.2841	18.8926
	0.25	18.8935	24.0937	33.1316	34.2692	27.7795	20.7572
	0.5	20.5907	26.2580	36.1079	37.3476	30.2750	22.6218
	0.75	22.2879	28.4223	39.0841	40.4260	32.7704	24.4864
	1.0	23.9851	30.5867	42.0603	43.5044	35.2658	26.3510
0.75	0.0	15.8868	20.2594	27.8591	28.8156	23.3587	17.4539
	0.25	17.4547	22.2589	30.6087	31.6596	25.6641	19.1765
	0.5	19.0227	24.2585	33.3583	34.5036	27.9695	20.8992
	0.75	20.5907	26.2580	36.1079	37.3476	30.2750	22.6218
	1.0	22.1586	28.2575	38.8574	40.1916	32.5804	24.3444
1.0	0.0	14.7626	18.8258	25.8878	26.7766	21.7058	16.2188
	0.25	16.2196	20.6839	28.4428	29.4194	23.8481	17.8196
	0.5	17.6766	22.5419	30.9978	32.0621	25.9904	19.4203
	0.75	19.1336	24.4000	33.5528	34.7049	28.1327	21.0211
	1.0	20.5907	26.2580	36.1079	37.3476	30.2750	22.6218

axial power-law index "k" enhances the beam's rigidity, leading to a corresponding rise in the critical buckling load, much like the influence of the transverse power-law index "p".

4.2.3 Small scale effect

Table 3 provides the dimensionless buckling load related to the nonlocal parameter "μ" and the length scale parameter "λ" for different FG nanobeams. To further illustrate these effects, Fig. 5 depicts the influence of the nonlocal parameter "μ" on the dimensionless critical buckling load for hardcore and softcore nanobeams. This parameter significantly affects the mechanical behavior of the beam, as an increase in "μ" results in a reduction in stiffness. Consequently, the critical buckling load decreases, irrespective of the nanobeam configuration or type.

To examine the effect of the length scale parameter "λ", Fig. 6 is presented. It is observed that "λ" has an inverse impact compared to the nonlocal parameter "μ". Increasing the length scale

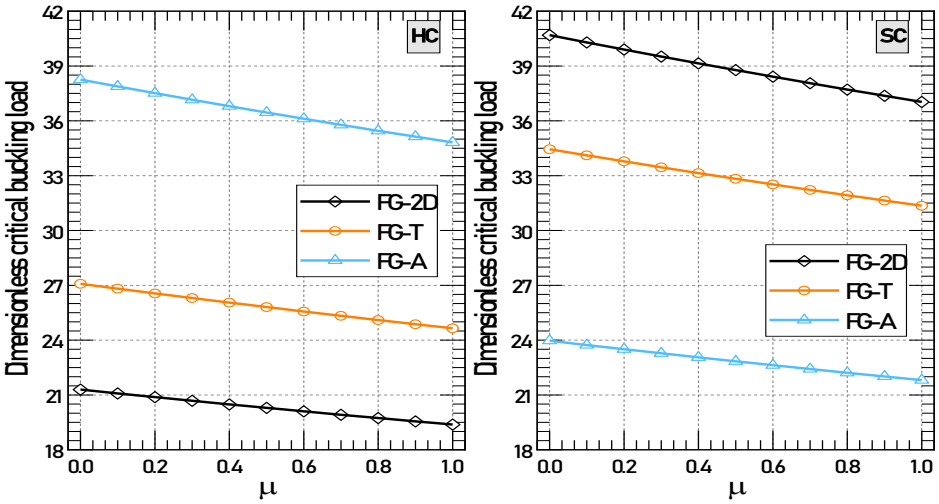

Fig. 5 Dimensionless buckling load versus the nonlocal parameter "μ" (SS, p=k=2, L/h=10, λ=0)

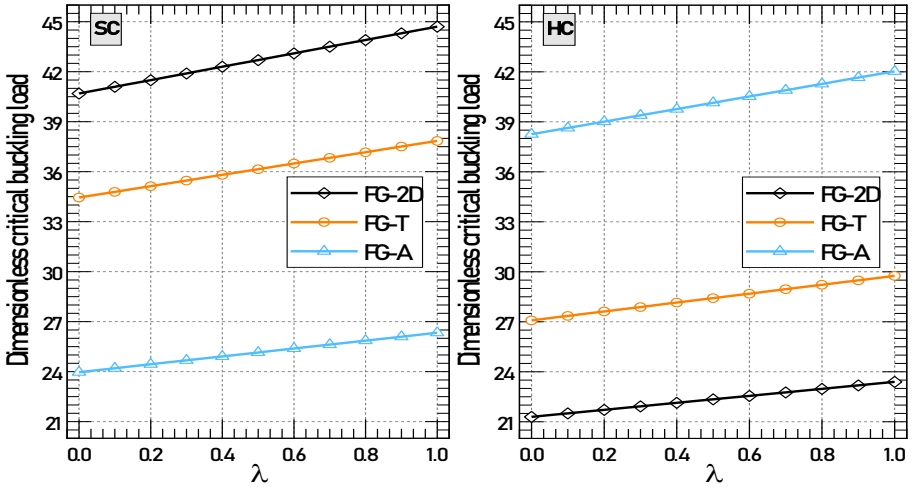

Fig. 6 Dimensionless buckling load versus the length scale parameter "λ" (SS, p=k=2, L/h=10, μ=0)

parameter enhances the beam's stiffness, leading to a higher critical buckling load.

4.2.4 Thickness ratio effect

Table 4 and Fig. 7 present the dimensionless buckling load as a function of the thickness ratio "L/h" for various boundary conditions. An increase in the thickness ratio leads to a corresponding rise in the dimensionless critical buckling load. Additionally, fully clamped beams require higher loads to buckle compared to other boundary conditions, highlighting their superior structural rigidity.

4.2.5 Elastic foundation effect

In this section, the elastic foundation parameters are represented in the following non-

Table 4 Dimensionless buckling load versus the thickness ratio "L/h" (SS, L/h=5, μ=λ=0)

P=k	L/h	HC			SC		
		FG-2D	FG-T	FG-A	FG-2D	FG-T	FG-A
2	5	20.5907	26.2580	36.1079	37.3476	30.2750	22.6218
	10	21.2902	27.0791	38.2507	40.6862	34.4457	23.9643
	15	21.4206	27.2313	38.6689	41.3646	35.3432	24.2263
	30	21.4990	27.3225	38.9231	41.7816	35.9038	24.3856
6	5	32.9028	36.8567	43.8142	25.1272	20.6082	14.9155
	10	34.3491	38.4588	46.4144	27.6519	23.3578	15.8006
	15	34.6241	38.7632	46.9218	28.1721	23.9467	15.9734
	30	34.7902	38.9470	47.2303	28.4932	24.3141	16.0784
8	5	35.8687	39.2066	45.0986	22.3054	18.6158	13.6311
	10	37.5461	41.0286	47.7750	24.4990	20.9029	14.4400
	15	37.8667	41.3766	48.2973	24.9500	21.3870	14.5979
	30	38.0606	41.5870	48.6148	25.2280	21.6879	14.6939
10	5	37.9438	40.8224	45.9159	20.3431	17.2346	12.8137
	10	39.7935	42.8044	48.6408	22.2864	19.2018	13.5742
	15	40.1482	43.1844	49.1726	22.6845	19.6140	13.7226
	30	40.3629	43.4144	49.4959	22.9298	19.8695	13.8128

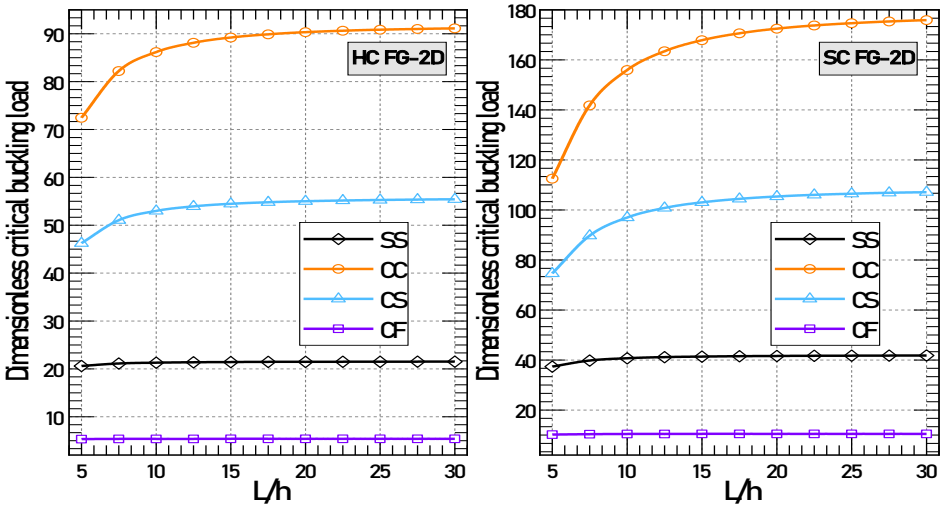

Fig. 7 Dimensionless critical buckling load versus the thickness ratio "L/h" (SS, p=k=2, μ=λ=0)

dimensional form

$$K_w = 10^2 \frac{k_w L^2}{A_{11}^0},\ K_g = 10^2 \frac{k_g}{A_{11}^0},\ K_L = 10^2 \frac{k_L L^2}{A_{11}^0},\ K_U = 10^2 \frac{k_U L^2}{A_{11}^0},\ K_S = 10^2 \frac{k_S}{A_{11}^0} \tag{53}$$

Here, the coefficient A_{11}^0 is of a beam made of pure metal, where

Table 5 Dimensionless buckling load versus the Winkler, Pasternak, and Kerr elastic foundation parameters (SS, L/h=5, μ=λ=0)

k_l	k_u	k_s	k_g=1			k_g=5			k_g=10		
			k_w=1	k_w=5	k_w=10	k_w=1	k_w=5	k_w=10	k_w=1	k_w=5	k_w=10
1	1	1	26.0367	39.2236	55.7071	27.3729	40.5597	57.0432	29.0430	42.2298	58.7133
		5	32.6302	45.8170	62.3005	33.9663	47.1531	63.6366	35.6364	48.8232	65.3067
		10	40.8719	54.0587	70.5422	42.2080	55.3948	71.8783	43.8781	57.0650	73.5485
	5	1	27.2470	40.4338	56.9173	28.5831	41.7699	58.2534	30.2532	43.4400	59.9236
		5	38.2360	51.4228	67.9063	39.5721	52.7589	69.2424	41.2422	54.4290	70.9126
		10	51.9723	65.1591	81.6426	53.3084	66.4952	82.9787	54.9785	68.1653	84.6488
	10	1	27.5220	40.7089	57.1924	28.8581	42.0450	58.5285	30.5283	43.7151	60.1986
		5	39.5101	52.6969	69.1804	40.8462	54.0330	70.5165	42.5163	55.7031	72.1866
		10	54.4951	67.6819	84.1654	55.8312	69.0180	85.5015	57.5013	70.6881	87.1716
5	1	1	25.0492	38.2360	54.7195	26.3853	39.5721	56.0556	28.0554	41.2422	57.7258
		5	27.2470	40.4338	56.9173	28.5831	41.7699	58.2534	30.2532	43.4400	59.9236
		10	29.9942	43.1811	59.6646	31.3303	44.5172	61.0007	33.0005	46.1873	62.6708
	5	1	26.7048	39.8916	56.3751	28.0409	41.2277	57.7112	29.7110	42.8978	59.3814
		5	33.2982	46.4850	62.9685	34.6343	47.8211	64.3046	36.3044	49.4913	65.9748
		10	41.5400	54.7268	71.2103	42.8761	56.0629	72.5464	44.5462	57.7330	74.2165
	10	1	27.5326	40.7194	57.2029	28.8687	42.0555	58.5390	30.5388	43.7257	60.2092
		5	36.3238	49.5106	65.9941	37.6599	50.8467	67.3302	39.3300	52.5169	69.0004
		10	47.3128	60.4996	76.9832	48.6489	61.8357	78.3193	50.3191	63.5059	79.9894
10	1	1	24.8247	38.0116	54.4951	26.1608	39.3477	55.8312	27.8310	41.0178	57.5013
		5	26.0235	39.2104	55.6939	27.3596	40.5465	57.0300	29.0298	42.2166	58.7001
		10	27.5220	40.7089	57.1924	28.8581	42.0450	58.5285	30.5283	43.7151	60.1986
	5	1	26.4337	39.6205	56.1040	27.7698	40.9566	57.4401	29.4399	42.6267	59.1103
		5	30.8293	44.0161	60.4996	32.1654	45.3522	61.8357	33.8355	47.0224	63.5059
		10	36.3238	49.5106	65.9941	37.6599	50.8467	67.3302	39.3300	52.5169	69.0004
	10	1	27.5399	40.7267	57.2102	28.8760	42.0628	58.5463	30.5461	43.7329	60.2164
		5	34.1333	47.3201	63.8036	35.4694	48.6562	65.1397	37.1395	50.3263	66.8098
		10	42.3750	55.5618	72.0454	43.7111	56.8979	73.3815	45.3813	58.5681	75.0516

$$A_{11}^{0} = \int_{-h/2}^{h/2}\int_{0}^{L}\left[\frac{E_m}{1-\upsilon^2}\right]dxdz \tag{54}$$

Table 5 presents the influence of the Winkler, Pasternak, and Kerr elastic foundations on the dimensionless critical buckling load, with each foundation parameter ranging from 1 to 10. Figs. 8 and 9 plot the impact of these parameters on beam stability to provide a more detailed physical interpretation.

Fig. 8 illustrates the influence of the Winkler and Pasternak elastic foundation parameters, denoted by "k_w" and "k_g", on the dimensionless critical buckling load. Including these parameters

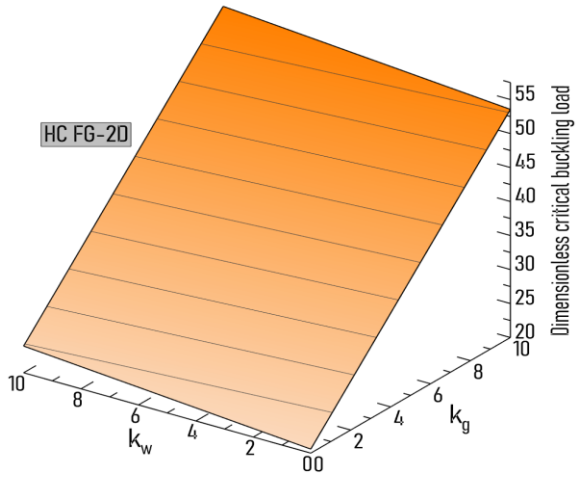

Fig. 8 Dimensionless critical buckling load versus Winkler/Pasternak elastic foundation parameters (SS, p=k=2, μ=λ=0)

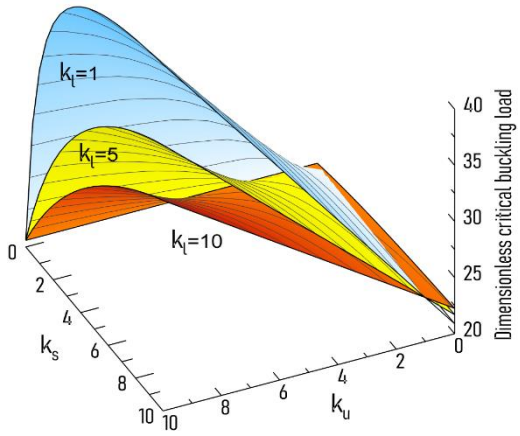

Fig. 9 Dimensionless critical buckling load versus Kerr elastic foundation parameters (SS, p=k=2, μ=λ=0)

enhances the beam's stiffness, leading to an increase in the buckling load. Notably, the Pasternak parameter "k_g" has a more pronounced effect, further reinforcing the structural stability of the beam.

Fig. 9 illustrates the influence of the Kerr elastic foundation parameters, denoted by "k_l", "k_u" and "k_s", on the dimensionless critical buckling load. The inclusion of these parameters enhances the beam's stiffness, contributing to an increase in the buckling load. Notably, an increase in "k_u" results in a linear rise in the critical buckling load, whereas "k_s" induces a nonlinear variation, highlighting the distinct mechanical effects of each parameter.

5. Conclusions

This paper investigated the buckling behavior of FG nanobeams with different material

distributions, resting on an elastic foundation modeled using the Winkler, Pasternak, and Kerr theories. A refined three-variable shear deformation theory incorporating a correction factor was developed, with displacement fields formulated based on Euler-Bernoulli beam theory. The nonlocal strain gradient elasticity theory was employed to account for small-scale effects. Galerkin-based solution approach was implemented to handle different boundary conditions. The study provided a comprehensive parametric analysis, evaluating the effects of material distribution, elastic foundation parameters, nonlocal effects, and geometric ratios on the critical buckling loads of FG nanobeams.

- The FG-A nanobeam, which features axial material distribution, is independent of the transverse power-law index, leading to constant buckling loads regardless of the beam scheme (hardcore or softcore).
- An increase in the transverse power-law index enhances beam stiffness in Hardcore FG-2D and FG-T configurations, requiring higher loads for buckling, with FG-T being more affected than FG-2D. Similarly, the axial power-law index follows the same trend, where its increase improves rigidity and raises the critical buckling load
- The nonlocal parameter significantly affects the mechanical response, where an increase in reduces beam stiffness, leading to a decrease in critical buckling loads.
- The length scale parameter has an opposite effect to the nonlocal parameter, as its increase enhances beam stiffness, raising the critical buckling load.
- A higher thickness ratio increases the dimensionless critical buckling load, and fully clamped beams exhibit greater resistance to buckling than other boundary conditions.
- The inclusion of the elastic foundation enhances beam rigidity, leading to an increase in the critical buckling load.

References

Akgöz, B. and Civalek, Ö. (2012), "Analysis of micro-sized beams for various boundary conditions based on the strain gradient elasticity theory", *Arch. Appl. Mech.*, **82**, 423-443. https://doi.org/10.1007/s00419-011-0565-5.

Belarbi, M.O., Benounas, S., Li, L., Van Vinh, P. and Garg, A. (2025), "Vibration of a functionally graded doubly curved shallow nanoshell: An improved FSDT model and its nonlocal finite element implement", *J. Vib. Eng. Technol.*, **13**(1), 93. https://doi.org/10.1007/s42417-024-01733-1.

Belarbi, M.O., Li, L., Ahmed Houari, M.S., Garg, A., Chalak, H.D., Dimitri, R. and Tornabene, F. (2022), "Nonlocal vibration of functionally graded nanoplates using a layerwise theory", *Math. Mech. Solid.*, **27**(12), 2634-2661. https://doi.org/10.1177/10812865221078571.

Belkacem, A., Ladmek, M., Daikh, A.A., Bessaim, A., Houari, M.S.A., Belarbi, M.O., ... & Tounsi, A. (2023), "Bending responses of bi-directional advanced composite nanobeams using higher order nonlocal strain gradient theory", *J. Nano Res.*, **79**, 77-90. https://doi.org/10.4028/p-56ju8c.

Bezzina, S., Bessaim, A., Houari, M.S.A. and Azab, M. (2022), "A new quasi-3D plate theory for free vibration analysis of advanced composite nanoplates", *Steel Compos. Struct.*, **45**(6), 830-850. https://doi.org/10.12989/scs.2022.45.6.830.

Carrera, E. (1999), "A study of transverse normal stress effect on vibration of multilayered plates and shells", *J. Sound Vib.*, **225**(5), 803-829. https://doi.org/10.1006/jsvi.1999.2271.

Chen, D., Zheng, S., Wang, Y., Yang, L. and Li, Z. (2020), "Nonlinear free vibration analysis of a rotating two-dimensional functionally graded porous micro-beam using isogeometric analysis", *Eur. J. Mech. A/Solid.*, **84**, 104083. https://doi.org/10.1016/j.euromechsol.2020.104083.

Chen, Y., Qian, S., Tang, H., Lai, X., Liu, Z., Han, S. and Jia, J. (2023), "Longlora: Efficient fine-tuning of

long-context large language models", arXiv preprint arXiv:2309.12307. https://doi.org/10.48550/arXiv.2309.12307.

Daikh, A.A., Belarbi, M.O., Khechai, A., Li, L., Ahmed, H.M. and Eltaher, M.A. (2023), "Buckling of bi-coated functionally graded porous nanoplates via a nonlocal strain gradient quasi-3D theory", *Acta Mechanica*, **234**(8), 3397-3420. https://doi.org/10.1007/s00707-023-03548-9.

Daikh, A.A., Houari, M.S.A. and Eltaher, M.A. (2021), "A novel nonlocal strain gradient quasi-3D bending analysis of sigmoid functionally graded sandwich nanoplates", *Compos. Struct.*, **262**, 113347. https://doi.org/10.1016/j.compstruct.2020.113347.

Daikh, A.A., Houari, M.S.A., Belarbi, M.O., Mohamed, S.A. and Eltaher, M.A. (2022), "Static and dynamic stability responses of multilayer functionally graded carbon nanotubes reinforced composite nanoplates via quasi-3D nonlocal strain gradient theory", *Def. Technol.*, **18**(10), 1778-1809. https://doi.org/10.1016/j.dt.2021.09.011.

Drai, A., Daikh, A.A., Belarbi, M.O., Houari, M.S.A., Aour, B., Hamdi, A. and Eltaher, M.A. (2023), "Bending of axially functionally graded carbon nanotubes reinforced composite nanobeams", *Adv. Nano Res.*, **14**(3), 211-224. https://doi.org/10.12989/anr.2023.14.3.211.

Ebrahimi, F. and Barati, M.R. (2018), "Buckling analysis of nonlocal strain gradient axially functionally graded nanobeams resting on variable elastic medium", *Proc. Inst. Mech. Eng., Part C*, **232**(11), 2067-2078. https://doi.org/10.1177/0954406217713518.

Ekinci, K. and Roukes, M. (2005), "Nanoelectromechanical systems", *Rev. Scientif. Instrum.*, **76**(6), 061101. https://doi.org/10.1063/1.1927327.

Eltaher, M.A., Emam, S.A. and Mahmoud, F.F. (2013), "Static and stability analysis of nonlocal functionally graded nanobeams", *Compos. Struct.*, **96**, 82-88. https://doi.org/10.1016/j.compstruct.2012.09.030.

Eltaher, M.A., Khairy, A., Sadoun, A.M. and Omar, F.A. (2014), "Static and buckling analysis of functionally graded Timoshenko nanobeams", *Appl. Math. Comput.*, **229**, 283-295. https://doi.org/10.1016/j.amc.2013.12.072.

Eringen, A.C. (1983), "On differential equations of nonlocal elasticity and solutions of screw dislocation and surface waves", *J. Appl. Phys.*, **54**(9), 4703-4710. https://doi.org/10.1063/1.332803.

Ermis, M., Dorduncu, M. and Kutlu, A. (2024), "Peridynamic differential operator for stress analysis of imperfect functionally graded porous sandwich beams based on refined zigzag theory", *Appl. Math. Model.*, **133**, 414-435. https://doi.org/10.1016/j.apm.2024.05.032.

Fang, F., Ran, S., Fang, Z., Song, P. and Wang, H. (2019), "Improved flame resistance and thermo-mechanical properties of epoxy resin nanocomposites from functionalized graphene oxide via self-assembly in water", *Compos. Part B: Eng.*, **165**, 406-416. https://doi.org/10.1016/j.compositesb.2019.01.086.

Ghandourah, E.E., Daikh, A.A., Alhawsawi, A.M., Fallatah, O.A. and Eltaher, M.A. (2022), "Bending and buckling of FG-GRNC laminated plates via quasi-3D nonlocal strain gradient theory", *Math.*, **10**(8), 1321. https://doi.org/10.3390/math10081321.

Ghandourah, E.E., Daikh, A.A., Khatir, S., Alhawsawi, A.M., Banoqitah, E.M. and Eltaher, M.A. (2023), "A dynamic analysis of porous coated functionally graded nanoshells rested on viscoelastic medium", *Math.*, **11**(10), 2407. https://doi.org/10.3390/math11102407.

Hetényi, M. (1946), *Beams on Elastic Foundation*, University of Michigan Press, Ann Arbor.

Houari, M.S.A., Bakoura, A., Belhocine, A., Younsi, A., Daikh, A.A., Belarbi, M.O. and Aid, A. (2025), "Analysis of buckling behavior in advanced sandwich composite beams using a novel hyperbolic shear deformation theory", *Adv. Aircraft Spacecraft Sci.*, **12**(2), 141-159. https://doi.org/10.12989/aas.2025.12.2.141.

Jamshidi, M., Arghavani, J. and Maboudi, G. (2019), "Post-buckling optimization of two-dimensional functionally graded porous beams", *Int. J. Mech. Mater. Des.*, **15**, 801-815. https://doi.org/10.1007/s10999-019-09443-3.

Karamanlı, A. (2017), "Bending behaviour of two directional functionally graded sandwich beams by using a quasi-3D shear deformation theory", *Compos. Struct.*, **174**, 70-86.

https://doi.org/10.1016/j.compstruct.2017.04.046.
Karamanlı, A. (2018), "Free vibration analysis of two directional functionally graded beams using a third order shear deformation theory", *Compos. Struct.*, **189**, 127-136. https://doi.org/10.1016/j.compstruct.2018.01.060.
Karamanli, A. (2023), "Transient vibration analysis of strain gradient multi-directional functionally graded microplates under a moving concentrated load", *Compos. Struct.*, **308**, 116678. https://doi.org/10.1016/j.compstruct.2023.116678.
Karamanli, A. and Vo, T.P. (2018), "Size dependent bending analysis of two directional functionally graded microbeams via a quasi-3D theory and finite element method", *Compos. Part B: Eng.*, **144**, 171-183. https://doi.org/10.1016/j.compositesb.2018.02.030.
Karamanli, A. and Vo, T.P. (2021), "Bending, vibration, buckling analysis of bi-directional FG porous microbeams with a variable material length scale parameter", *Appl. Math. Model.*, **91**, 723-748. https://doi.org/10.1016/j.apm.2020.09.058.
Karamanli, A., Wattanasakulpong, N., Lezgy-Nazargah, M. and Vo, T.P. (2023), "Bending, buckling and free vibration behaviours of 2D functionally graded curved beams", *Struct.*, **55**, 778-798. https://doi.org/10.1016/j.istruc.2023.06.052
Kerr, A.D. (1964), "Elastic and viscoelastic foundation models", *J. Appl. Mech.*, **31**(3), 491-498. https://doi.org/10.1115/1.3629667.
Kolahchi, R., Bidgoli, A.M.M. and Heydari, M.M. (2015), "Size-dependent bending analysis of FGM nano-sinusoidal plates resting on orthotropic elastic medium", *Struct. Eng. Mech.*, **55**(5), 1001-1014. https://doi.org/10.12989/sem.2015.55.5.1001.
Ladmek, M., Belkacem, A., Houari, M.S.A., Daikh, A.A., Bessaim, A., Belarbi, M.O., ... & Eltaher, M.A. (2023), "On vibration responses of advanced functionally graded carbon nanotubes reinforced composite nanobeams", *J. Nano Res.*, **80**, 49-63. https://doi.org/10.4028/p-u9eXPt.
Li, L., Hu, Y. and Ling, L. (2015), "Flexural wave propagation in small-scaled functionally graded beams via a nonlocal strain gradient theory", *Compos. Struct.*, **133**, 1079-1092. https://doi.org/10.1016/j.compstruct.2015.08.014.
Lim, C.W., Zhang, G. and Reddy, J. (2015), "A higher-order nonlocal elasticity and strain gradient theory and its applications in wave propagation", *J. Mech. Phys. Solid.*, **78**, 298-313. https://doi.org/10.1016/j.jmps.2015.02.001.
Mohamed, I., Kahya, V. and Şimşek, S. (2025), "A new higher-order finite element model for free vibration and buckling of functionally graded sandwich beams with porous core resting on a two-parameter elastic foundation using quasi-3D theory", *Iran. J. Sci. Technol., Trans. Civil Eng.*, **49**(1), 383-408. https://doi.org/10.1007/s40996-024-01482-x.
Mohamed, I., Kahya, V. and Şimşek, S. (2025), "Finite element static analysis of functionally graded sandwich beams with porous core resting on a two-parameter elastic foundation based on quasi-3D theory", *Proc. Inst. Mech. Eng., Part C: J. Mech. Eng. Sci.*, **239**(6), 2129-2149. https://doi.org/10.1177/09544062241297120.
Mohamed, I., Kahya, V. and Şimşek, S. (2025), "Ritz-type quasi-3D solution for free vibration and buckling of functionally graded sandwich beams with porous core resting on a two-parameter elastic foundation", *Arab. J. Sci. Eng.*, **50**(16), 13343-13367. https://doi.org/10.1007/s13369-024-09729-5.
Mohamed, I., Şimşek, S. and Kahya, V. (2025), "Free vibration and buckling analysis of functionally graded sandwich beams resting on a two-parameter elastic foundation using a quasi-3D theory", *Sigma J. Eng. Nat. Sci.*, **43**(1), 47-61.
Mohamed, I., Şimşek, S., Kahya, V. and Lanc, D. (2024), "Computational modeling of functionally graded sandwich beams with porous core using an Ansys APDL-based approach", *Mech. Bas. Des. Struct. Mach.*, **53**(6), 4337-4358. https://doi.org/10.1080/15397734.2024.2448715.
Mouffoki, A., Azab, M., Aicha, B., Belhocine, A., Aicha, R., Daikh, A.A., ... & Tounsi, A. (2025), "A novel integral parabolic plate theory incorporating stretching effects for the bending analysis of advanced FG plates resting on Winkler-Pasternak foundations", *Couple. Syst. Mech.*, **14**(5), 451-472. https://doi.org/10.12989/csm.2025.14.5.451.

Mouffoki, A., Bedia, E.A., Houari, M.S.A., Tounsi, A. and Mahmoud, S.R. (2017), "Vibration analysis of nonlocal advanced nanobeams in hygro-thermal environment using a new two-unknown trigonometric shear deformation beam theory", *Smart Struct. Syst.*, **20**(3), 369-383. https://doi.org/10.12989/sss.2017.20.3.369.

Nguyen, V.C., Tran, H.Q. and Pham, V.V. (2025), "The role of partial elastic foundations on the bending and vibration behaviors of bi-directional hybrid functionally graded nanobeams using FEM", *Arch. Appl. Mech.*, **95**(1), 1-25. https://doi.org/10.1007/s00419-024-02708-0.

Pasternak, P. (1954), *On a New Method of an Elastic Foundation by Means of Two Foundation Constants*, Gosudarstvennoe Izdatelstvo.

Rahmani, O., Refaeinejad, V. and Hosseini, S.A.H. (2017), "Assessment of various nonlocal higher order theories for the bending and buckling behavior of functionally graded nanobeams", *Steel Compos. Struct.*, **23**(3), 339-350. https://doi.org/10.12989/scs.2017.23.3.339.

Reddy, J.N. (1984), "A simple higher-order theory for laminated composite plates", *J. Appl. Mech.*, **51**(4), 745-752. https://doi.org/10.1115/1.3167719.

Remil, A., Belarbi, M.O., Bessaim, A., Houari, M.S.A., Bouamoud, A., Daikh, A.A., ... & Eltaher, M.A. (2023), "An accurate analytical model for the buckling analysis of FG-CNT reinforced composite beams resting on an elastic foundation with arbitrary boundary conditions", *Comput. Concrete*, **31**(3), 267-276. https://doi.org/10.12989/cac.2023.31.3.267.

Remil, A., Benrahou, K.H., Draiche, K., Bousahla, A.A. and Tounsi, A. (2019), "A simple HSDT for bending, buckling and dynamic behavior of laminated composite plates", *Struct. Eng. Mech.*, **70**(3), 325-337. https://doi.org/10.12989/sem.2019.70.3.325.

Rizov, V. (2017), "Analysis of longitudinal cracked two-dimensional functionally graded beams exhibiting material non-linearity", *Fract. Struct. Integr.*, **11**(41), 491-503. https://doi.org/10.3221/IGF-ESIS.41.61.

Sayyad, A.S., Hadji, L. and Tounsi, A. (2023), "On the mechanics of FG nanobeams: A review with numerical analysis", *Forc. Mech.*, **12**, 100219. https://doi.org/10.1016/j.finmec.2023.100219.

Selvadurai, A.P. (1979), *Elastic Analysis of Soil-Foundation Interaction*, Elsevier.

Tharwan, M.Y., Daikh, A.A., Assie, A.E., Alnujaie, A. and Eltaher, M.A. (2025), "Size-dependent buckling of multidirectional porous metal foam nanoshells resting on an orthotropic elastic foundation", *Arch. Civil Mech. Eng.*, **25**(1), 1-22. https://doi.org/10.1007/s43452-024-01074-6.

Trinh, L.C., Nguyen, H.X., Vo, T.P. and Nguyen, T.K. (2016), "Size-dependent behaviour of functionally graded microbeams using various shear deformation theories based on the modified couple stress theory", *Compos. Struct.*, **154**, 556-572. https://doi.org/10.1016/j.compstruct.2016.07.033.

Turan, M. and Adiyaman, G. (2024), "Free vibration and buckling analysis of porous two-directional functionally graded beams using a higher-order finite element model", *J. Vib. Eng. Technol.*, **12**(1), 1133-1152. https://doi.org/10.1007/s42417-023-00898-5.

Turan, M., Kahya, V., Yaylaci, E.U. and Yaylaci, M. (2025), "A shear deformable numerical approach for the static analysis of bi-directional functionally graded beams", *Adv. Nano Res.*, **18**(2), 143-162. https://doi.org/10.12989/anr.2025.18.2.143.

Vinh, P.V., Belarbi, M.O. and Tounsi, A. (2022), "Wave propagation analysis of functionally graded nanoplates using nonlocal higher-order shear deformation theory with spatial variation of the nonlocal parameters", *Wave. Random Complex Media.*, **35**(1), 1-21. https://doi.org/10.1080/17455030.2022.2036387.

Vo, T.P., Thai, H.T., Nguyen, T.K., Maheri, A. and Lee, J. (2014), "Finite element model for vibration and buckling of functionally graded sandwich beams based on a refined shear deformation theory", *Eng. Struct.*, **64**, 12-22. https://doi.org/10.1016/j.engstruct.2014.01.029.

Winkler, E. (1867), *Die Lehre von der Elasticitaet und Festigkeit*, Dominicus, Prag.

Xin, L. and Kiani, Y. (2023), "Vibration characteristics of arbitrary thick sandwich beam with metal foam core resting on elastic medium", *Struct.*, **49**, 1-11. https://doi.org/10.1016/j.istruc.2023.01.108.

Xu, X.J., Wang, X.C., Zheng, M.L. and Ma, Z. (2017), "Bending and buckling of nonlocal strain gradient elastic beams", *Compos. Struct.*, **160**, 366-377. https://doi.org/10.1016/j.compstruct.2016.10.038.

Yamanouti, M. and Koizumi, M. (1990), *Proceedings of the First International Symposium on Functionally*

Gradient Materials (FGM'90), Sendai, Japan.
Yang, T., Tang, Y., Li, Q. and Yang, X.D. (2018), "Nonlinear bending, buckling and vibration of bi-directional functionally graded nanobeams", *Compos. Struct.*, **204**, 313-319. https://doi.org/10.1016/j.compstruct.2018.07.045.
Zghal, S. and Dammak, F. (2020), "Vibrational behavior of beams made of functionally graded materials by using a mixed formulation", *Proc. Inst. Mech. Eng., Part C: J. Mech. Eng. Sci.*, **234**(18), 3650-3666. https://doi.org/10.1177/0954406220916533.